Modeling and Simulation of Si IGBTs

N. Shigyo[1], M. Watanabe[1], K. Kakushima[1], T. Hoshii[1], K. Furukawa[1],
A. Nakajima[2], K. Satoh[3], T. Matsudai[4], T. Saraya[5], T. Takakura[5], K. Itou[5],
M. Fukui[5], S. Suzuki[5], K. Takeuchi[5], I. Muneta[1], H. Wakabayashi[1],
S. Nishizawa[6], K. Tsutsui[1], T. Hiramoto[5], H. Ohashi[1] and H. Iwai[1]
E-mail: n.shigyo@i.softbank.jp
[1]Tokyo Institute of Technology, [2]Nat. Inst. Advanced Industrial Science and Technology,
[3]Mitsubishi Electric Corp., [4]Toshiba Electronic Devices & Storage Corp.,
[5]The University of Tokyo, [6]Kyushu University

***Abstract*— Technology CAD (TCAD) has been recognized as a powerful design tool for Si insulated gate bipolar transistors (IGBTs). Here, physical models, such as a mobility model for carrier-carrier scattering, were investigated for a predictive TCAD. Simulated current-voltage characteristics of the trench-gate IGBTs were compared with measurements. The difference between 3D- and 2D-TCAD simulations was observed in a high current region, which was explained by a bias-dependent current flow. A test element group (TEG) for separation of the emitter currents for holes and electrons was also determined as effective for calibration of lifetime model parameters.**

Keywords—IGBT, trench-gate, TCAD simulation, carrier-carrier scattering, three-dimension current flow, injection enhancement effect

I. Introduction

High-efficiency power electronic systems are necessary for worldwide energy saving. A power device acts as a high voltage power switch in such systems. Therefore, the three main requirements for the power device are a low on-resistance R_{on}, a low switching loss and a sufficient safe operating area (SOA) such as a breakdown voltage.

Basic concepts of Si insulated gate bipolar transistors (IGBTs) were developed in the early 1980s [1]-[3]. Lowering of the on-state voltage V_{CEsat} was achieved by introducing electron injection enhancement (IE) effect for a trench-gate IGBT with non-latch-up structure [4]. Many improvements for IGBTs have been made, which was reviewed in [5]-[7]. Although there has been significant progress with wide bandgap materials such as SiC and GaN [8]-[11], IGBTs will still have an important role for the next years [5]-[7].

Technology CAD (TCAD), especially device simulation, has contributed to improvements in IGBTs [12]. A scaling concept for IGBTs was proposed using TCAD simulations [13], taking the relations between IE effect and scaling scheme into considerations. The first IGBT designed by the scaling scheme was experimentally confirmed [14]-[16]. 3300 V IGBTs were driven by a 5 V gate voltage, which enabled the use flexible and intelligent power control schemes due to its CMOS compatibility [16].

This work was based on results obtained from the project (JPNP10022) commissioned by the New Energy and Industrial Technology Development Organization (NEDO).
N. Shigyo is now with Kioxia Corporation.

It is well-known that there are tradeoffs among the three stated requirements [5]-[7], [17], [18]. A predictive TCAD is required to analyze tradeoffs and optimize IGBTs. In previous studies [19], good agreements were found between simulations and measurements for trench-gate IGBTs in the *low*-current region, close to V_{CEsat}. In the *high*-current region, only a few studies have been reported that compare the current-voltage characteristics, e.g. [20]. The authors elucidated the difference between 3D- and 2D-simulations for trench-gate IGBTs [21], so that excellent agreement was obtained between 3D-simulations and measurements of the current-voltage characteristics. The importance of 3D-simulation was confirmed in [22], where simulated transient turn-off behavior was also agreed well with measurements.

In this paper, physical models are investigated to achieve predictive TCAD, and a comparison between 3D-simulations and measurements of the current-voltage characteristics is described. A test element group (TEG) [23] for separation of the emitter currents for holes and electrons is described, which provided detailed information on the IGBTs and enabled advances for calibration of model parameters.

II. Basic Operation of IGBT

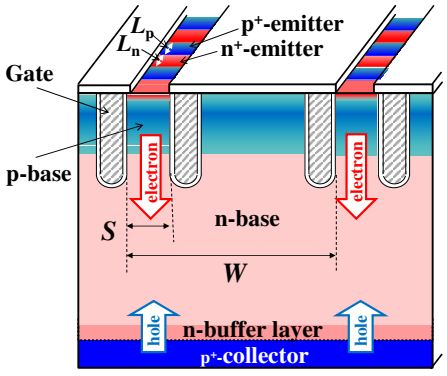

Fig. 1 Schematic diagram of trench-gate IGBT structure.

Fig. 1 shows the basic structure of the trench-gate IGBT [4], where W is the pitch, S is the mesa width between trenches, and L_n and L_p are the lengths of the n^+- and p^+-emitters, respectively.

The IGBT is a combination of a Si power MOSFET and a bipolar junction transistor (BJT). Electrons are injected into the n-base region by the MOSFET. The injected electrons cause the bottom pn junction to turn on. Holes are then

injected into the n-base region from the p⁺-collector (back emitter), which results in a large amount of electron-hole plasma in the n-base region. Both electrons and holes contribute to the current flow, so that a low R_{on} is a feature of the IGBT.

III. Physical Models for IGBT Simulation

Selection of the appropriate physical model is essential for predictive TCAD. The IGBT is a combination of a MOSFET and a BJT, so that models for an intrinsic carrier concentration n_i and a bandgap narrowing ΔE_g^{app} were examined, since these models are important for the BJT simulation [24]. A mobility model for carrier-carrier scattering μ_{cc} proposed by Klaassen [25] was also investigated, because the IGBT was operated in the presence of the electron-hole plasma. This μ_{cc} model considers the attractive interaction potential for electron-hole scattering. The Synopsys TCAD software [26] was used for the simulations.

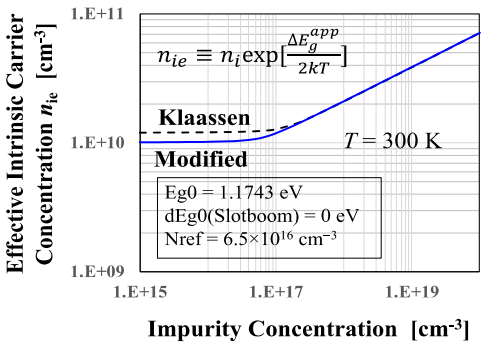

Fig. 2 Models for effective intrinsic carrier concentration n_{ie}.

Fig. 2 shows the effective intrinsic carrier concentration n_{ie} as a function of the impurity concentration. The model for ΔE_g^{app} is coupled with that for n_i [24]. ΔE_g^{app} proposed by Klaassen et al. [27] was based on an n_i of 1.20×10^{10} cm^{-3} at T = 300 K. Here, the model for ΔE_g^{app} was modified to accord with an n_i of 1.00×10^{10} cm^{-3} at T = 300 K proposed by Sproul and Green [28]. The modified parameters are given in the inset of Fig. 2.

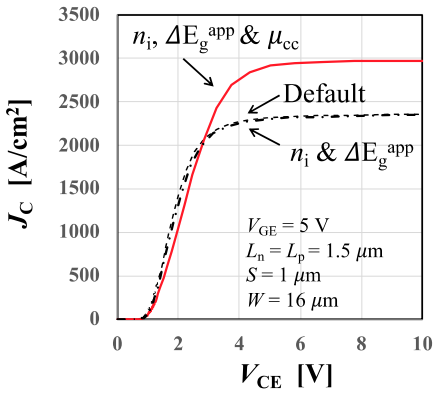

Fig. 3 Influence of physical models (n_i, ΔE_g^{app} and μ_{cc}) on J_C-V_C characteristics.

Fig. 3 shows the influence of the physical model on the J_C-V_{CE} characteristics, where J_C is the collector current density and V_{CE} is the collector-emitter voltage. The change in J_C caused by n_i and ΔE_g^{app} was less than 1%, even under BJT operation. The adoption of μ_{cc} resulted in a decrease in the mobility. However, the collector saturation current J_{Csat}, was increased by 26%. These results are explained as follows.

J_{Csat} consists of the electron and hole current densities, J_e and J_h, which are approximated by the drift current in the n-base region. Thus, J_{Csat} is expressed as

$$J_{Csat} \simeq q(n\mu_e + p\mu_h)\, E \qquad (1)$$

where q is the elementary charge, n and p are the electron and hole densities, respectively, μ_e and μ_h are the respective electron and hole mobilities, and E is the electric field in the n-base region. In the high current region, J_e is mainly determined by the electron supply, i.e., the drain saturation current I_{Dsat} of the MOSFET:

$$I_{Dsat} = qn\mu_e E A_C \qquad (2)$$

where A_C is the collector area. Thus, the product of nE is expressed as

$$nE = I_{Dsat}/(q\mu_e A_C). \qquad (3)$$

The adoption of μ_{cc} resulted in the decrease in μ_e, so that the nE product in the n-base region was increased to satisfy (2), i.e., $I_{Dsat} = J_e A_C$. With consideration of the carrier plasma ($p \simeq n$), (1) can be rewritten using (3);

$$J_{Csat} \simeq (1 + \mu_h/\mu_e) I_{Dsat}/A_C. \qquad (4)$$

The μ_{cc} caused an increase in J_h, and therefore J_{Csat}, because the decrease in μ_h was smaller than that in μ_e due to the larger hole effective mass m_h^* compared with m_e^*.

The influence of n_i and ΔE_g^{app} on the J_C-V_{CE} characteristics was negligibly small, because J_e is determined by the drain current I_D of the MOSFET for $J_C > J_{on}$, where J_{on} is the on-state current density. Understanding both the IGBT operation and physical models is thus required for predictive TCAD.

A TEG was developed to monitor the minority carrier lifetime τ_h in the n-base region [29]. The current-voltage characteristics for two diodes consisting of p⁺-emitter and n-base regions were used, so that τ_h can be measured using the same IGBT wafer.

IV. Comparisons with Measurements

The simulated current-voltage characteristics for the trench-gate IGBTs were compared with measurements.

A. *Difference between 3D- and 2D-simulations*

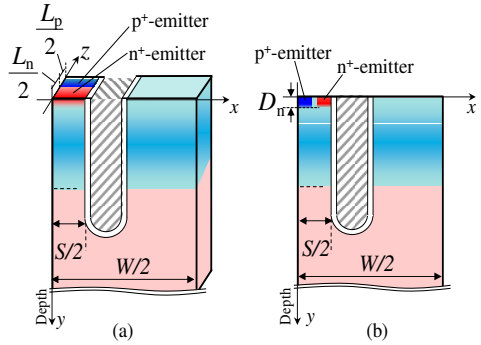

Fig. 4 Half-cell models for (a) 3D- and (b) 2D-device simulations of trench-gate IGBT.

Figs. 4(a) and (b) show half-cell models for the 3D- and 2D-simulations, respectively. The most notable difference between the two models is the structure of the n^+- and p^+-emitters at the top of the mesa. For the 3D-model, the n^+- and p^+-emitters with lengths L_n and L_p are placed alternately, where $L_n + L_p$ is the pitch of the emitter structure. For the 2D-simulation, the p^+-emitter is embedded in the same plane as the n^+-emitter.

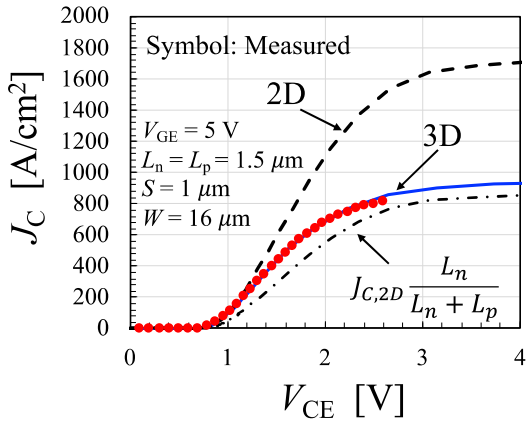

Fig. 5 J_C-V_{CE} characteristics calculated by 3D- and 2D-simulations, and corresponding measurements.

Fig. 5 shows the J_C-V_{CE} characteristics obtained by 3D- and 2D-simulations, and those from the corresponding measurements [14] for a scaling factor $k = 3$ and $L_n = L_p = 1.5$ µm. Here, the resistances of the contact and substrate were taken into account [21]. The 3D-simulation results revealed excellent agreement with the measurements for a wide range of J_C up to 1000 A/cm^2. However, the 2D-simulation reproduced the measurement only for J_C < 100 A/cm^2. In the high-current region, J_C appeared to be well fitted by the expression $J_{C,2D} \cdot L_n/(L_n + L_p)$, where $J_{C,2D}$ is J_C obtained by the 2D-simulations.

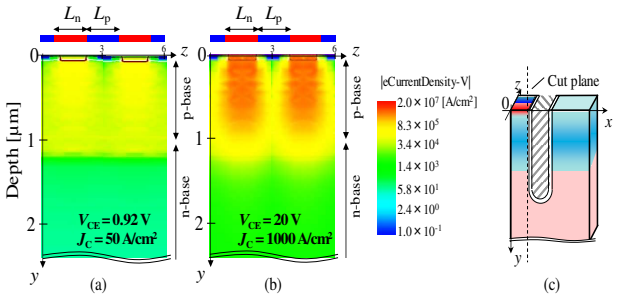

Fig. 6 3D-simulated distribution of electron current density in vertical direction $|J_{ey}|$ on cross-section close to channel surface for V_{GE} = 5 V. (a) J_C = 50 A/cm^2, (b) $J_C = J_{Csat}$ =1000 A/cm^2, (c) position of cross-section.

Fig. 6 shows the distribution of the electron current density component $|J_{ey}|$, for the cross-section close to the channel surface. When J_C was less than J_{on} (= 200 A/cm^2), the electric field in the channel was low because the potential difference between the n^+-emitter and n-base regions was small. Therefore, the injected electrons were distributed uniformly in the channel, as shown in Fig. 6(a). This situation was similar to the 2D-simulation, although the emitter structures were significantly different between the 3D- and 2D-simulations. However, in the high-current region ($J_C = J_{Csat}$), electrons were injected only from the n^+-emitter, as shown in Fig. 6(b). In this situation, J_C was limited by the electron supply from the MOSFET. Therefore, J_C could be approximated by $J_{C,2D} \cdot L_n/(L_n + L_p)$, as shown in Fig. 5.

Application of the 2D-simulations was limited to only the low-current region for the IGBTs, because of the bias-dependent 3D current flow and carrier distribution.

B. Measurement for electron and hole emitter currents

For the trench-gate IGBT, the on-state voltage V_{CEsat} becomes lower with a reduction of the mesa width S. The holes injected from the p^+-collector reach the mesa region surrounded by trenches, so that the hole current flow is restricted. The positively charged holes thus enhance electron injection into the n-base region to satisfy charge neutrality, which is referred to as the IE effect [4]. A TEG was fabricated for direct measurement of the IE effect [23].

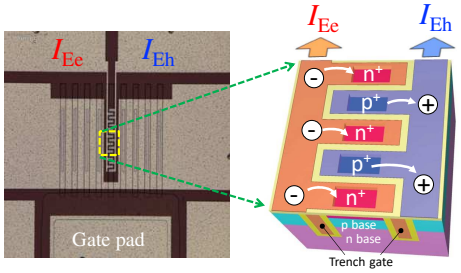

Fig. 7 (a) Plane view of IGBT after fabrication and (b) schematic view of contact arrangement for current-separating emitter.

Fig. 7(a) shows a plan-view image of the TEG, where two separated interdigitated electrodes for the emitter are in contact with each n^+ and p^+ region to allow for independent measurement of the emitter currents for electrons I_{Ee} and holes I_{Eh}, as shown in Fig. 7(b).

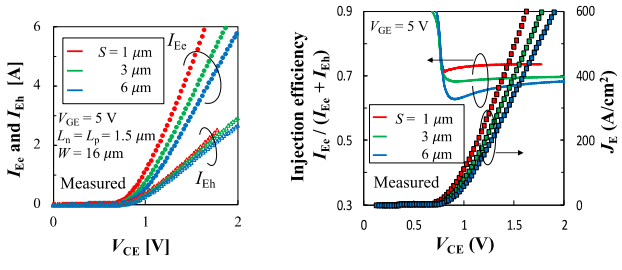

Fig. 8 (a) Measured emitter electron current I_{Ee} and emitter hole current I_{Eh}, and (b) electron injection efficiency $I_{Ee}/(I_{Eh} + I_{Eh})$ (solid lines) and J_E-V_{CE} characteristics (symbols) with various mesa width S.

Figs. 8(a) and (b) show the measured I_{Ee} and I_{Eh} as a function of V_{CE}, and the electron injection efficiency and J_E-V_{CE} characteristics for IGBTs with different mesa widths S, respectively. Fig. 8(a) demonstrates that the increase in I_{Ee} was greater than that in I_{Eh} as S decreased, although both I_{Ee} and I_{Eh} increased. As a result, the electron injection efficiency clearly increased as S narrowed, as shown in Fig. 8(b). This provides direct evidence of the IE effect. In addition, Fig. 8(b)

confirms that V_{CEsat} was reduced due to the decrease in S. I_E for low V_{CE} also consisted mostly of I_{Ee}.

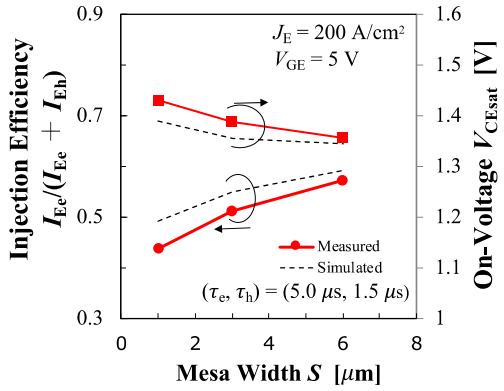

Fig. 9. Electron injection efficiency $I_{Ee}/(I_{Ee} + I_{Eh})$, and on-state voltage V_{CEsat} as function of mesa width S at J_E = 200 A/cm².

Fig. 9 shows the dependence of the electron injection efficiency and V_{CEsat} on S at J_E = 200 A/cm². The fact that the injection efficiency increases and V_{CEsat} decreases as S is reduced, was consistent with the 3D simulation results.

The individual evaluations of I_{Ee} and I_{Eh} were an additional constraint condition for calibration of the lifetime in the n-base region, where a τ_e of 5.0 µs and a τ_h of 1.5 µs were determined. The information for I_{Ee} and I_{Eh} would thus facilitate TCAD calibration.

V. Conclusion

Excellent agreement of the current-voltage characteristics between measurements and TCAD simulations was obtained for trench-gate IGBTs. The adoption of the mobility model for carrier-carrier scattering resulted in an increase in the collector current density J_C, even though the mobility was reduced. The difference between the 3D- and 2D-TCAD simulations in the high-current region could be explained by the bias-dependent 3D-current flow and carrier distribution. The TEG to separate the emitter currents for holes and electrons was determined to be effective for calibration of the lifetime model parameter.

Acknowledgment

The authors would like to thank Prof. I. Omura and Prof. M. Tsukuda of Kyushu Institute of Technology and Prof. W. Saito of Kyushu Univ. for fruitful discussions.

This work was based on results obtained from the project (JPNP10022) commissioned by the New Energy and Industrial Technology Development Organization (NEDO).

References

[1] J. D. Plummer, "Monolithic semiconductor switching device," U.S. Patent 4199774, Apr. 22, 1980.

[2] H. W. Becke and C. F. Wheatley, Jr., "Power MOSFET with an anode region," U.S. Patent 4364073, Dec. 14, 1982.

[3] A. Nakagawa et al., "Non-luchup 1200 V 75 A bipolar mode ASO," *Tech. Dig. IEDM* 1984, pp. 860-861.

[4] M. Kitagawa et al., "A 4500 V injection enhanced insulated gate bipolar transistor (IEGT) operating in a mode similar to a thyristor," *Tech. Dig. IEDM* 1993, pp. 679–682.

[5] N. Iwamuro and T. Laska, "IGBT history, state-of-the-art, and future prospects," *IEEE Transactions on Electron Devices*, vol. 64, pp. 741-752, 2017.

[6] N. Iwamuro and T. Laska, "Correction to "IGBT history, state-of-the-art, and future prospects"," *IEEE Trans. on Electron Devices*, vol. 65, p. 2675-2675, 2018.

[7] T. Laska, "Progress in Si IGBT technology – as on going competition with WBG power devices," *Tech. Dig. IEDM* 2019, pp. 262-265.

[8] J. W. Palmour, "Silicon carbide power device development for industrial markets," *Tech. Dig. IEDM* 2014, pp. 1.1.1-1.1.8.

[9] J. B. Casady et al., "New generation 10kV SiC power MOSFET and Diodes for Industrial Applications," *Proceedings of PCIM Europe 2015*, pp. 1–8.

[10] D. Marcon, Y. N. Saripalli, and S. Decoutere, "200mm GaN-on-Si epitaxy and e-mode device technology," *Tech. Dig. IEDM* 2015, pp. 16.2.1-16.2.4.

[11] Y. Zhang et al., "Reduction of on-resistance and current crowding in quasi-vertical GaN power diodes," *Applied Physics Letters*, vol. 111, no. 16, pp. 163-506, 2017.

[12] H. Ohashi and I. Omura, "Role of simulation technology for the progress in power devices and their applications," *IEEE Trans. on Electron Devices*, vol.60, pp. 528 - 534, 2013.

[13] M. Tanaka and I. Omura, "IGBT scaling principle toward CMOS compatible wafer processes," *Solid-State Electronics*, vol. 80, pp. 118–123, 2013.

[14] K. Kakushima et al., "Experimental verification of a 3D scaling principle for low Vce(sat) IGBT," *Tech. Dig. IEDM* 2016, pp. 10.6.1-10.6.4.

[15] T. Saraya et al., "Demonstration of 1200V scaled IGBTs driven by 5V gate voltage with superiorly low switching loss,", *Tech. Dig. IEDM 2018*, pp. 8.4.1-8.4.4.

[16] T. Saraya et al., "3300 V scaled IGBTs driven by 5 V gate voltage," *Proc., ISPSD* 2019, pp. 43-46.

[17] K. Satoh et al., "New chip design technology for next generation power module," *Proc. PCIM* 2008, p.673.

[18] K. Nishi, T. Takahashi and A. Narazaki, "Analysys the complex tradeoff among E_{on}-V_{CEsat}-SCSOA and EMI noise through the single chip evaluation method," *Proc., ISPSD* 2019, pp. 475-478.

[19] P. Luo et al., "Numerical analysis of 3-dimensional scaling rules on a 1.2-kV trench clustered IGBT," *IEEE Tran. Electron Devices*, vol. 65, no. 4, pp. 1440-1446, 2018.

[20] H. Feng et al., "A 1200 V-class fin p-body IGBT with ultra-narrow mesas for low conduction loss," *Proc., ISPSD* 2016, pp. 203-205.

[21] M. Watanabe et al., "Impact of three-dimensional current flow on accurate TCAD simulation for trench-gate IGBTs," *Proc., ISPSD* 2019, pp. 311-314.

[22] T. Suwa and S. Hayase, "Investigation of TCAD calibration for saturation and tail current of 6.5kV IGBTs," *Proc., SISPAD* 2019, pp. 101-104

[23] T. Hoshii et al., "Verification of the injection enhancement effect in IGBTs by measuring the electron and hole currents separately," *Proc. ESSDERC 2018*, pp. 26-29.

[24] N. Shigyo, N. Konishi and H. Satake, "An improved bandgap narrowing model based on corrected intrinsic carrier concentration," *Trans. IEICE,* vol. E75-C, pp. 156-160, 1992.

[25] D. B. M. Klaassen, "Unified mobility model for device simulation," *Solid-St. Electron.*, vol. 35, pp. 953-959, 1992.

[26] TCAD Sentaurus User Manual, Version M-2016.12, Synopsys, San Jose, CA, USA, 2016.

[27] D. B. M. Klaassen, J. W. Slotboom and H. C. de Graaf, "Unified apparent bandgap narrowing in n and p-type silicon," *Solid-St. Electron.*, vol. 35, pp. 125-129, 1992.

[28] A. B. Sproul and M. A. Green, "Improved value for the silicon intrinsic carrier concentration from 275 to 375 K," *J. Appl. Phys.*, vol. 70, pp. 846-854, 1991.

[29] K. Kakushima et al., "New methodology for evaluating minority carrier lifetime for process assessment," *Proc. of Symposia on VLSI Technology and Circuits* 2018, pp. 105-106.